Accepted Manuscript

Title: A magnetically separable SO_4/Fe-Al-TiO_2 solid acid catalyst for biodiesel production from waste cooking oil

Authors: Jabbar Gardy, Amin Osatiashtiani, Oscar Céspedes, Ali Hassanpour, Xiaojun Lai, Adam F. Lee, Karen Wilson, Mohammad Rehan

PII: S0926-3373(18)30375-8
DOI: https://doi.org/10.1016/j.apcatb.2018.04.046
Reference: APCATB 16617

To appear in: *Applied Catalysis B: Environmental*

Received date: 24-12-2017
Revised date: 13-4-2018
Accepted date: 18-4-2018

Please cite this article as: Gardy J, Osatiashtiani A, Céspedes O, Hassanpour A, Lai X, Lee AF, Wilson K, Rehan M, A magnetically separable SO_4/Fe-Al-TiO_2 solid acid catalyst for biodiesel production from waste cooking oil, *Applied Catalysis B: Environmental* (2010), https://doi.org/10.1016/j.apcatb.2018.04.046

A magnetically separable SO_4/Fe-Al-TiO_2 solid acid catalyst for biodiesel production from waste cooking oil

Jabbar Gardy[1], Amin Osatiashtiani[2], Oscar Céspedes[3], Ali Hassanpour[1, *], Xiaojun Lai[1, *], Adam F. Lee[4], Karen Wilson[4], Mohammad Rehan[5]

[1] School of Chemical and Process Engineering, University of Leeds, West Yorkshire, Leeds, LS2 9JT, UK.
[2] European Bioenergy Research Institute, Aston University, Aston Triangle, Birmingham, B4 7ET, UK
[3] School of Physics and Astronomy, University of Leeds, West Yorkshire, Leeds, LS2 9JT, UK
[4] School of Science, RMIT University, Melbourne VIC3001, Australia.
[5] Centre of Excellence in Environmental Studies (CEES), King Abdulaziz University, Jeddah, Saudi Arabia.
[*]Tel: +44(0)113 343 2405; E-mail (A.H.): a.hassanpour@leeds.ac.uk; (X.L.): x.lai@leeds.ac.uk

Graphical abstract

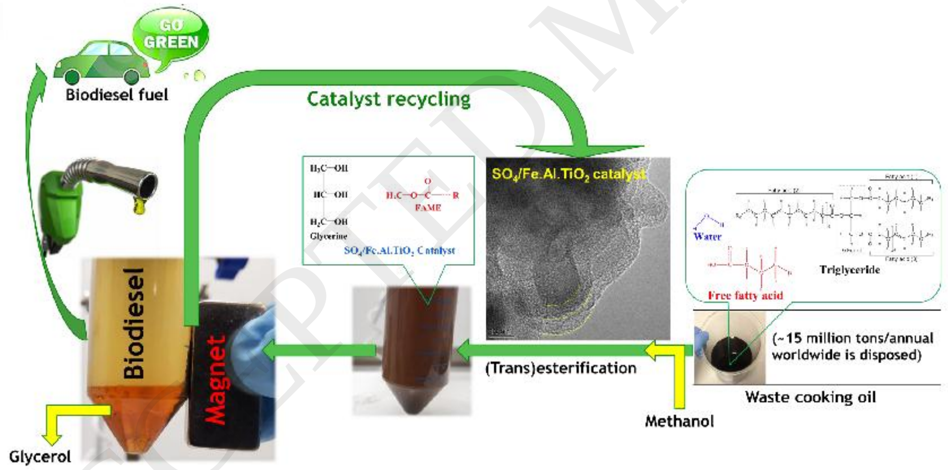

Research highlights

- A novel super paramagnetic solid acid nano-catalyst [SO_4/Fe-Al-TiO_2] was synthesised
- We examined the catalytic activity, stability and reusability of SO_4/Fe-Al-TiO_2

- 95.6% of FAME yield was achieved from WCO using newly developed nano-catalyst
- Synthesised biodiesel from WCO satisfied ASTM D6751 and EN 14214 standards

Abstract

A novel magnetic SO_4/Fe-Al-TiO_2 solid acid catalyst was synthesized for biodiesel production via the (trans)esterification of waste cooking oil (WCO). The nanocomposite catalyst was prepared by the sequential functionalisation of commercial rutile/anatase mixed phase TiO_2 nanoparticles (NPs) with alumina as a buffer layer, and subsequently hematite to impart magnetic character, prior to sulfation with chlorosulfonic acid to introduce Brønsted acidity. XRD showed that the SO_4/Fe-Al-TiO_2 catalyst comprised titania (rutile and anatase phases), aluminium sulphate, and hematite nanoparticles, while electron microscopy revealed the layer-by-layer assembly of these components within the SO_4/Fe-Al-TiO_2 catalyst. FTIR confirmed the presence of surface sulphate groups SO_4^{2-} and $S_2O_7^{2-}$/$S_3O_{10}^{2-}$, creating a predominantly Brønsted acid catalyst with high acid loading. The catalyst achieved 96 % fatty acid methyl ester (FAME) yield from WCO after 2.5 h of reaction at 90 °C, using 3 wt% of the magnetic catalyst, and a methanol:oil molar ratio of 10:1. SO_4/Fe-Al-TiO_2 was also effective for feedstocks containing up to 20 wt% of free fatty acid (FFA), and showed excellent stability for WCO (trans)esterification over 10 recycles.

Keywords

Solid acid catalyst; (trans)esterification; magnetic nanoparticle; biodiesel; waste cooking oil

1. Introduction

Developing alternative fuel has attracted a growing interest over the past twenty five years due to the depletion of fossil fuels, human health hazards and climate change [1, 2]. Biodiesel, which comprises fatty acid alkyl esters (FAMEs) is gaining popularity as an alternative fuel because of its availability, being eco-friendly, non-toxicity and biodegradability [3, 4]. Currently around 90% of the worldwide biodiesel in industry is being produced by homogenous acid/alkaline catalyzed (trans)esterification process of triglycerides in oleaginous food crops with methanol [5]. However, using these food oil crops would require significant amounts of freshwater and arable lands. This could also lead to food security problems in developing countries [6]. Waste(used) cooking oil [7], (micro)algae [8], and jatropha seeds [9] could be used as alternative non-food source feedstocks to overcome the aforementioned issue for the production of cheap biodiesel fuel. Nevertheless, such raw materials for biodiesel production contain a high level of free fatty acids (FFA) resulting in soap (fatty acid salts) formation [10]. Therefore, design of heterogeneous catalysts, as alternative to homogeneous catalysts currently used in the industrial synthesis of biodiesel fuel, has been the subject of intensive research to overcome this problem [11].

Solid acid catalyst design has received considerable attention for biodiesel production from cheap and non-food feedstocks. This is because solid acid catalysts can simultaneously perform esterification of FFAs and transesterification of triglycerides without (1) soap formation, (2) corrosion of the reactors, (3) quenching steps, and (4) neutralisation of by-products. They also allow for process intensification via continuous biodiesel production [12]. More importantly, the potential recovery and reusability of these catalysts from the (trans)esterification reaction make them preferable for industrial biodiesel production [13-16]. Numerous synthetic routes are emerging for the preparation of solid acid catalysts for different applications [17-33]. Sulfated metal oxides have been recently used as typical solid acid catalysts for the (trans)esterification process and we have also recently reported the synthesis of a novel titanium sulphate oxide [$Ti(SO_4)O$] catalyst for the (trans)esterification of waste cooking oil (WCO) to form biodiesel [5]. The incorporation of sulphate groups into metal oxides mainly enhance the Brønsted acidity property and catalytic activity [34-36]. However, low surface area and/or difficulty in the separation process of solid acid catalysts still persist main drawbacks [18, 30, 37-39]. Some researchers have reported that the presence of magnetic properties in catalysts increases their re-usability by enabling fast recovery with little loss using external magnetic fields [26, 40-43]. Magnetic properties in solid acid catalysts are an excellent mean for separating the catalyst from the reaction media but the surface of magnetic oxide materials are unstable under acidic conditions, being very sensitive compared to titania, and the particles can be easily aggregated into large clusters due to anisotropic dipolar interactions, which result in loss of their catalytic activity [44, 45]. Several methods have been introduced to overcome this issue, including a layer-by-layer coating of the surface with different metal oxides and polymers [28, 30, 39]. Therefore, it is necessary to develop a novel magnetic solid material as a potential catalyst candidate that could fulfil all requirements for the industrial (trans)esterification process. Here, we report, for the first time, the design and synthesis of a multifunctional magnetic solid acid [SO_4/Fe-Al-TiO_2] catalyst for the production of biodiesel from WCO. Characterisation and application investigations of this new designed magnetic solid acid catalyst for biodiesel production via (trans)esterification of WCO are carried out and reported.

2. Experimental

2.1 Materials

Aluminium iso-propoxide (+98 % granular, $Al(O\text{-}i\text{-}Pr)_3$) was purchased from Alfa Aesar whilst oleic acid (≥99 %), hydrochloric acid (37%, HCl) and chlorosulfonic acid (HSO_3Cl, 99%) were obtained from Fluka Analytical. Titanium (IV) oxide nanoparticles (99.5 %, product number 718467-100G), methanol (≥99.9 %), ethanol (≥99.8 %), ethylene glycol (99.8 %, EG), ammonium hydroxide (28-30 %, NH_4OH), ferric chloride hexahydrate (≥98 %, $FeCl_3.6H_2O$), ferrous chloride tetrahydrate (≥99.99 %, $FeCl_2.4H_2O$), (methyl heptadecanoate (≥99.5 %), n-heptane (≥99 %), acetone (99.9%) and n-hexane (99.5%) were purchased from Sigma-Aldrich. All chemicals were used without further purification. The sample of WCO was provided by a local restaurant in Leeds, was used as the feedstock for biodiesel production. The collected WCO was pre-treated by filtration and then heated at 100 °C for 5 h to reduce the water content; the resulting WCO contained 0.14 wt% moisture and 2 wt% FFA.

2.2 Catalyst preparation

The catalyst was synthesised via stepwise deposition of alumina and iron oxides on to commercial TiO_2 NPs. This is expected to both increase the surface area, and introduce magnetic character, the former should minimise mass transfer limitations by providing a large pore network for subsequent liquid phase catalysis [46]. The addition of alumina and iron oxides into the commercial TiO_2

catalyst should also improve the thermal stability, acidity of TiO_2 catalyst as well as catalytic activity as compared to previously used $Ti(SO_4)O$ [5] and sulphated Fe_2O_3/TiO_2 [47].

2.2.1 Synthesis of alumina coated TiO_2

0.1 mols of aluminium iso-propoxide was dispersed in a round-bottomed flask containing 50 ml of ethanol. Subsequently, 1 g of commercial TiO_2 NPs and 5 ml of ammonium hydroxide were added to the flask, and the resulting solution stirred at 250 rpm for 10 min. The resulting suspension was refluxed at 80 °C under vigorous stirring until a light yellowish gel formed. The solvent was then evaporated by ageing the solution without agitation at room temperature for 24 h, and the powder obtained then washed repeatedly with 1:1 vol% ethanol:deionised water. The aluminium impregnated TiO_2 was then oven-dried overnight at 100 °C, prior to static calcination in air at 400 °C for 5 h. This sample is denoted Al-TiO_2.

2.2.2 Preparation of iron oxide coated Al-TiO_2

The preceding Al-TiO_2 material was subsequently iron oxide functionalised through the co-precipitation of Fe^{2+} and Fe^{3+} precursors under alkaline conditions ($Fe^{2+} + 2\ Fe^{3+} + 8\ OH^- \rightarrow Fe_3O_4 + 4\ H_2O$ [48, 49]). 0.15 mols ferric chloride hexahydrate and 0.1 mols ferrous chloride tetrahydrate were separately dissolved in 50 ml of a 1:1 vol% ethanol:deionised water under ultrasonication until they formed clear solutions. The resulting solutions were both added dropwise to a three neck round-bottomed flask containing 2 g of Al-TiO_2 nanoparticles suspended in 50 ml of ethanol and 10 ml of ethylene glycol under stirring. 25 ml of concentrated ammonium hydroxide were injected into the reaction mixture until the pH reached 9-10. The reaction mixture was then heated to 75 °C under reflux and a N_2 atmosphere, and vigorously stirred for 2 h, followed by static ageing for 12 h. The gel obtained was separated using an external magnetic field, and rinsed repeatedly with 1:1 ethanol: deionised water until chloride ions could not be detected (using $AgNO_3$) in the washings. The resulting dark-reddish gel was then oven dried overnight at 80 °C, prior to calcination under static air at 400 °C for 4 h. This temperature chosen to be below the threshold to induce an anatase to rutile phase transition, [50] yet sufficient to form hematite. This sample is denoted Fe-Al-TiO_2.

2.2.3 Chlorosulfonic acid functionalization of Fe-Al-TiO_2

1 g of Fe-Al-TiO_2 was dispersed in 50 ml of dry toluene by ultrasonication. The suspension was then cooled to -5 °C using an ice bath, and gently stirred during the addition of 2 ml chlorosulfonic acid, injected at 0.1 $ml.min^{-1}$. The suspension was refluxed at 60 °C for 2 h under a N_2 atmosphere, and the resulting solid magnetically separated from the solution, thoroughly washed with fresh toluene until neutral washings were obtained, and then oven-dried overnight prior to calcination at 400 °C for 4 h. This sample, representing the final solid acid catalyst is denoted SO_4/Fe-Al-TiO_2. The overall catalyst synthesis is summarised in **Scheme 1**.

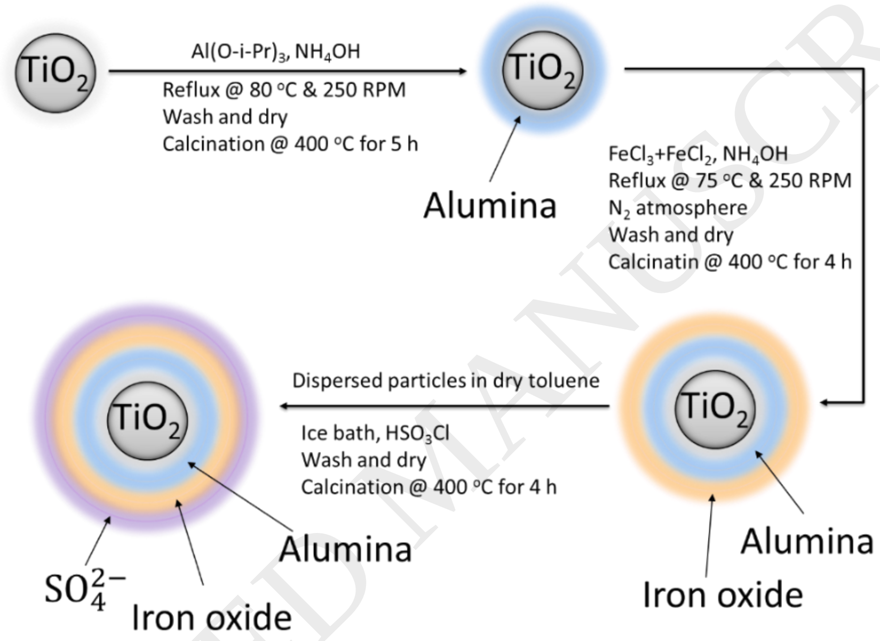

Scheme 1. Schematic of SO_4/Fe-Al-TiO_2 catalyst synthesis.

2.3 Catalyst characterisation

Sample crystallinity was explored by powder X-ray diffraction (XRD) using a Bruker D8 diffractometer and Cu Kα radiation (1.54 Å, 40 kV/40 mA) between 10 and 70 ° and steps of 0.0495° (35 s per step). Fourier transform infrared (FTIR) spectra were recorded at room temperature using a Nicolet iS10 spectrometer between 650 and 4000 cm^{-1} with a resolution of 4 cm^{-1}. Catalyst morphology and particle size distributions were examined using a cold field emission scanning electron microscopy (CFE-SEM, SU8230 Hitachi) operated at 1-2 kV, and scanning transmission electron microscopy (STEM, FEI Titan Themis Cubed 300) operated at 300 kV. Samples were dispersed in acetone over a carbon-coated copper grid. Elemental compositions and spatial distributions were determined by HAADF detector in conjunction with an energy dispersive

X-ray spectrometer (EDS, Oxford INCA 350). Nitrogen adsorption-desorption isotherms were measured on a Micromeritics TriStar 3000 porosimeter at 77 K, on samples degassed overnight at 120 °C in vacuo. Thermogravimetric analysis (TGA) was performed on a Mettler Toledo (TGA/DSC-1) stare system under N_2 gas at 50 ml.min^{-1} and a heating rate of 10 °C.min^{-1} from 25 to 900 °C. Brønsted/Lewis acid character was determined by diffuse reflectance IR spectroscopy (DRIFTS) on pyridine titrated samples. Prior to DRIFTS analysis, samples were diluted to 10 wt% in KBr, and pyridine adsorbed *ex-situ* by wetting samples with physisorbed pyridine removed in vacuo at 100 °C overnight. Spectra were collected at 50 °C on a Thermo Scientific Nicolet iS50 spectrometer using an environmental cell and Smart Collector accessory. Acid loadings were determined by TGA-MS through the thermal desorption of reactively formed propene, with samples first saturated with n-propylamine, and physisorbed n-propylamine removed in vacuo at 30 °C overnight. Analysis of untreated and n-propylamine treated samples was performed using a Mettler Toledo TGA/DSC-2 instrument connected via a heated capillary to a Pfeiffer ThermoStar mass spectrometer under flowing He at 30 ml.min^{-1} and a heating rate of 10 °C.min^{-1} from 40 to 800 °C. The amount and temperature at which reactively-formed propene (m/z=41) and ammonia (m/z=15) were evolved are respectively quantitative measures of the number and strength of acid sites at which n-propylamine chemisorbed. Magnetic properties were assessed on a Maglab 9T vibrating sample magnetometer (VSM, Oxford instruments) at room temperature. 10-15 mg of sample was accurately weighed into a gelatine capsule and loaded into the sample holder which was subsequently placed between pick-ups coils located in a He flow cryostat and sinusoidally vibrated. The centre of sample oscillation was first positioned at the vertical centre of the pick-up coils, and off-centre. The sample was held in a 2 Tesla magnetic field at room temperature, with the resulting change in magnetic flux induced within the coils and associated electromagnetic field (EMF) proportional to the magnetic moment (M) of the sample. Finally, the coercivity (H_c) and the remanence (M_r in unit Am^2) were determined from the magnetic moment/ external magnetic field curve.

2.4 Catalyst test

The (trans)esterification of WCO was conducted in a glass batch reactor equipped with a temperature controller, mechanical stirrer, and a reflux condenser. Specific amounts of SO_4/Fe-Al-TiO_2 catalyst, methanol and pre-treated WCO were charged to the reactor at room temperature. The solid-liquid-liquid phases were mixed under constant stirring and heated to the required temperature. After a specified time, the reaction mixture was subsequently transferred to a separating funnel and allowed to cool to room temperature. The FAME-containing layer was then separated from the residual catalyst by centrifugation at 9000 rpm for 10 min, and a few ml of the FAME then analysed by off-line GC-MS (580S, Perkin Elmer Clarus gas chromatograph, equipped with a 560S mass spectrometer) according to the modified ASTM and EU standard methods [5].

2.5 Biodiesel characterisation

The flash point of the produced biodiesel was measured by an auto ramp, closed cup, flash point tester (Setaflash series 3). The temperature was ramped at 1-2 °C.min^{-1} until the flash was captured. Biodiesel density at 15 °C was measured using the pycnometric method. A Bohlin-Gemini 150 rotary rheometer (Malvern, UK) was used to measure the biodiesel viscosity. Trace moisture content was analysed by volumetric Karl Fischer titration (Mettler Toledo-V20, Germany). The acid values and FFA% of the oil and synthesised biodiesel were measured according to standard methods [51, 52]. The acid value and the percentage of free fatty acid of biodiesel were calculated as follows:

$$\text{Acid value, mgKOH/g} = \frac{(V_{bs} - V_b) * C * 56.11}{W} \qquad \text{Eqn. (1)}$$

$$\text{Free fatty acid, \%} = \frac{(V_{bs} - V_b) * C * 28.246}{W} \qquad \text{Eqn. (2)}$$

Where: $V_{bs}$is consumed volume of titrate for the biodiesel sample in ml; V_b is consumed volume of titrate for the blank in ml; C is exact concentration of standardised alcoholic potassium hydroxide solution (mole/l) and W is mass of biodiesel sample used in g.

The biodiesel cloud point was determined using a differential scanning calorimetry (DSC 1, Mettler Toledo, UK) equipped with an intracooler system (Huber TC45): 5±2.5 mg of biodiesel sample was weighted in a 40 µl sealed aluminium pan and placed in the DSC sample chamber and heated to 50 °C at 1 °C.min^{-1} and held for 5 min to homogenise the sample should it contain any wax compounds. The system was then cooled to -30 °C at 1 °C.min^{-1} and held for 5 min, with onset temperature of the initial exothermic peak during cooling defined as the cloud point [12]. The sample was maintained under flowing nitrogen at 50 ml.min^{-1} throughout. Finally, the thermal stability of the biodiesel was assessed on a Stanton Redcroft thermogravimetric analyser (TGA-TGH 1000) on 20-25 mg of biodiesel sample which was heated from 25 to 600 °C at 10 °C.min^{-1} under flowing air at 50 ml.min^{-1}.

3. Results and discussion

3.1 Catalyst characterisation

3.1.1 Crystalline structure

The crystallinity of SO_4/Fe-Al-TiO_2 was explored through XRD, which revealed reflections characteristic of rhombohedral α-Fe_2O_3 (JCPDS-ICDD: 01-076-4579), rhombohedral aluminium sulphate (millosevichite, JCPDS-ICDD: 00-042-1428), and tetragonal titanium dioxide (anatase, JCPDS-ICDD: 04-006-9240 and rutile, JCPDS-ICDD: 01-076-9000) as shown in **Figure 1**. The sharp reflections of α-Fe_2O_3 and aluminium sulfate evidence a highly ordered (extended) hematite phase, while those for titania were far weaker/broader consistent with small crystallites. Corresponding volume-averaged crystallite sizes and *d*-spacings for the most intense reflection of each phase are given in **Table 1**.

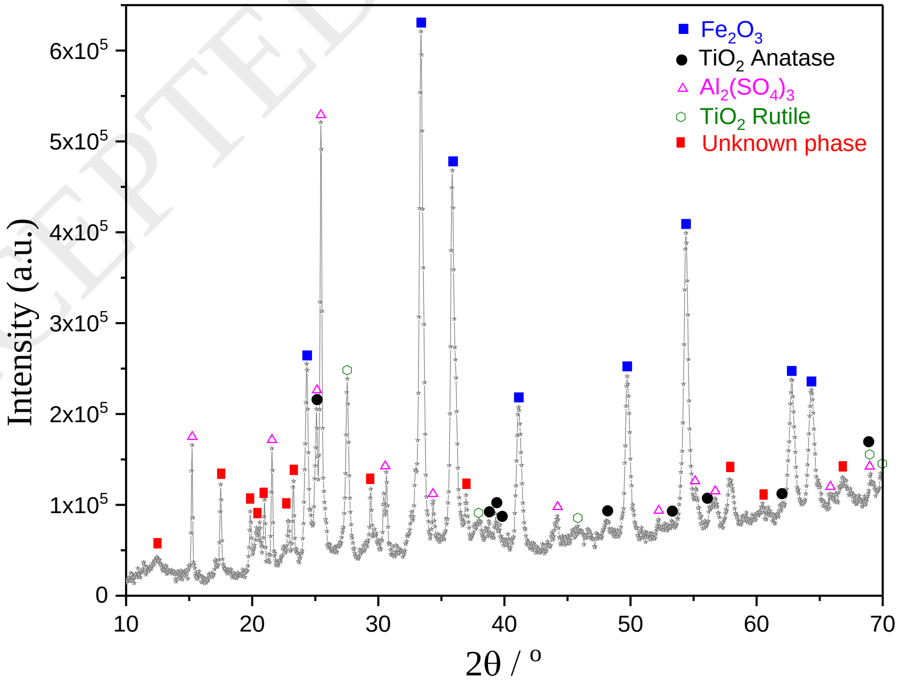

Figure 1. Powder XRD pattern of SO_4/Fe-Al-TiO_2 catalyst.

Table 1. Crystallite sizes and *d*-spacings for components of SO_4/Fe-Al-TiO_2.

Phase	**Reflection**	**2θ / °**	**FWHM / °**	***d*-spacing / Å**	**Crystallite size / nm**
Anatase	[101]	25.1	0.15	3.5	56
Rutile	[110]	27.5	0.19	3.2	42
α-Fe_2O_3	[104]	33.4	0.24	2.7	34
$Al_2(SO_4)_3$	[113]	25.4	0.15	3.5	56

3.1.2 Electron microscopy

SEM of the initial aluminium functionalised titania reveals agglomerates of approximately 50 nm spherical particles (**Figure S1**). Corresponding TEM reveals tetragonal and hexagonal particles, some of which exhibit a core-shell like (**Figure S2a**), with some evidence for anatase truncated octahedron crystallites terminating in [001]. The mean particle size was around 15-25 nm (**Figure S2b**). HRTEM and EDX analysis (**Figure 2**) is consistent with the formation of a low contrast amorphous alumina shell (**Figure S2a inset**), approximately 3 nm thick, encapsulating a denser titania core.

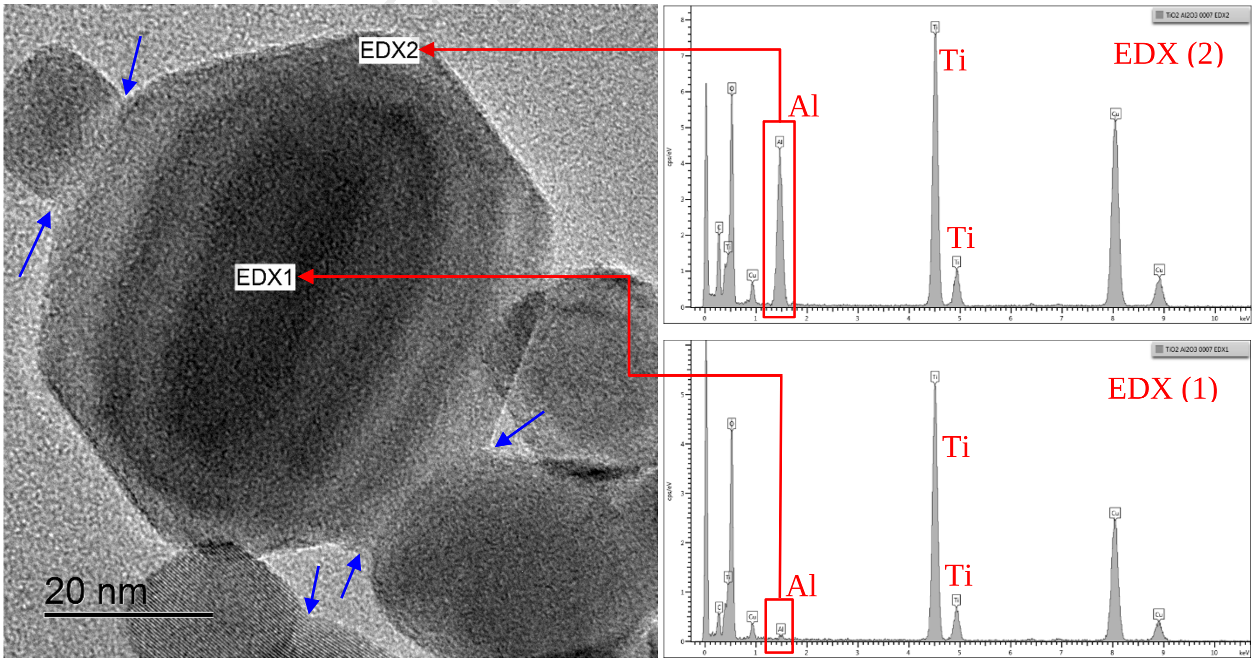

Figure 2. TEM-EDX spectra for a single particle shows the coating of alumina on the TiO_2 NPs. The blue arrows represent the oriented attachment of nanoparticles.

SEM (**Figure S3**) and TEM (**Figure S4**) images of the Al-TiO_2 material after iron oxide functionalisation (Fe-Al-TiO_2) again reveal dense agglomerates of ~50 nm diameter and irregular shape nanoparticles, some of which are decorated with very small (<10 nm) higher contrast nanoparticles which we attribute to hematite. Particle agglomeration may well reflect the magnetic character imparted by the iron oxide component. Elemental analysis (**Table 2**) of Fe-Al-TiO_2 reveals a near 1:1 Al:Ti atomic ratio (**Figure S5**), and Fe:Al ratio of 0.4 consistent with only partial decoration of the surface of the alumina encapsulated titania nanoparticles. EDS elemental maps of Fe-Al-TiO_2 are shown in **Figure 3**, demonstrate that Al and Fe are deposited as relatively homogenous shells around titania nanoparticles, illustrated in **Figure S6**.

Table 2. EDS elemental analysis of Fe-Al-TiO_2.

Element	**O**	**Ti**	**Al**	**Fe**
wt%	36.9	32.6	16.5	14.0

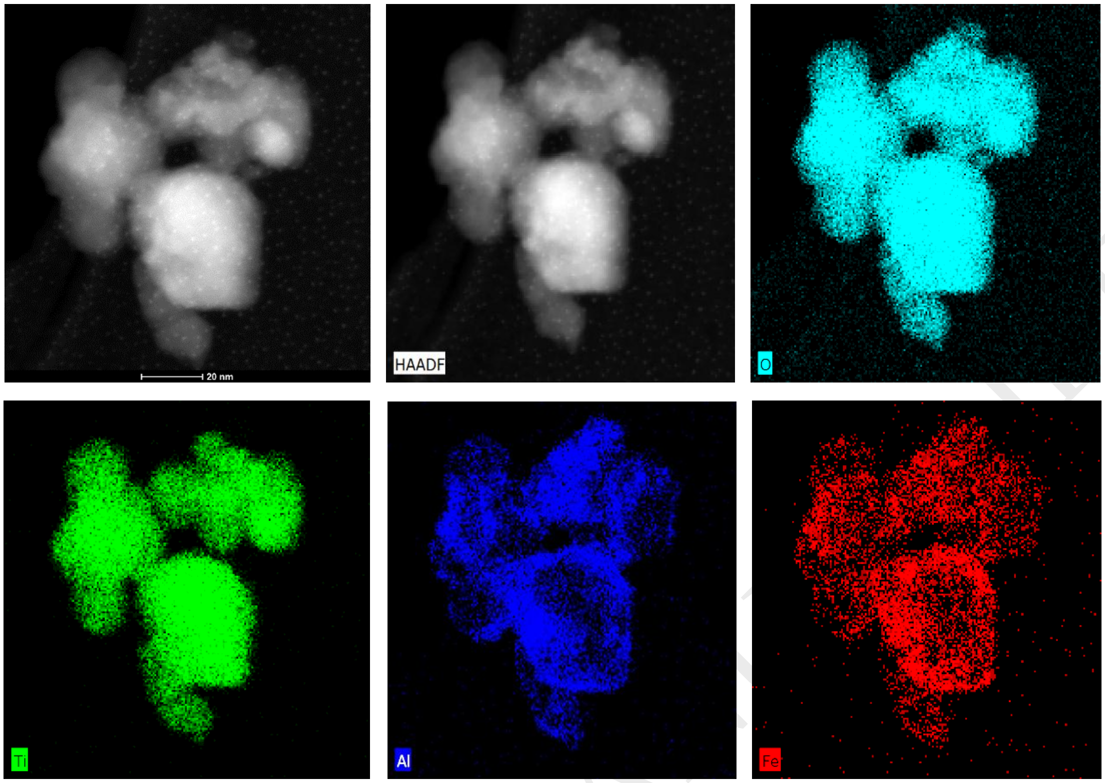

Figure 3. (clockwise from top left) Dark-field HAADF-STEM, and EDS elemental maps of O, Ti, Al, and Fe highlighting uniform distribution of each component in Fe-Al-TiO_2 catalyst.

The sulfonated Fe-Al-TiO_2 was subsequently examined by SEM (**Figure S7-9**) and TEM (**Figure 4**). SEM micrographs reveal little change in the morphology upon sulfonation, with dense aggregates of irregular shaped nanoparticles around 50 nm diameter visible. Corresponding TEM confirm the presence of a range of nanoparticle shape and size (<50 nm), with lattice fringes of 0.356 nm attributable to the rhombohedral millosevichite form of $Al_2(SO_4)_3$ (**Figure 4a**), [110] planes of anatase (**Figure 4b**), and [110] and [012] planes of rutile TiO_2 (**Figures 4c** and **e**) and rhombohedral hematite (**Figure 4e**). A SAED pattern confirmed the presence of all four crystalline phases within individual nanoparticles, in agreement with XRD. **Figure 4c-d** also provide further evidence that the core-shell structure of the parent Al-TiO_2 nanoparticles are retained following Fe and S modification, resulting in a uniform (~5 nm thick) shells comprising a mix of alumina, hemite and millosevichite encapsulating anatase and rutile cores.

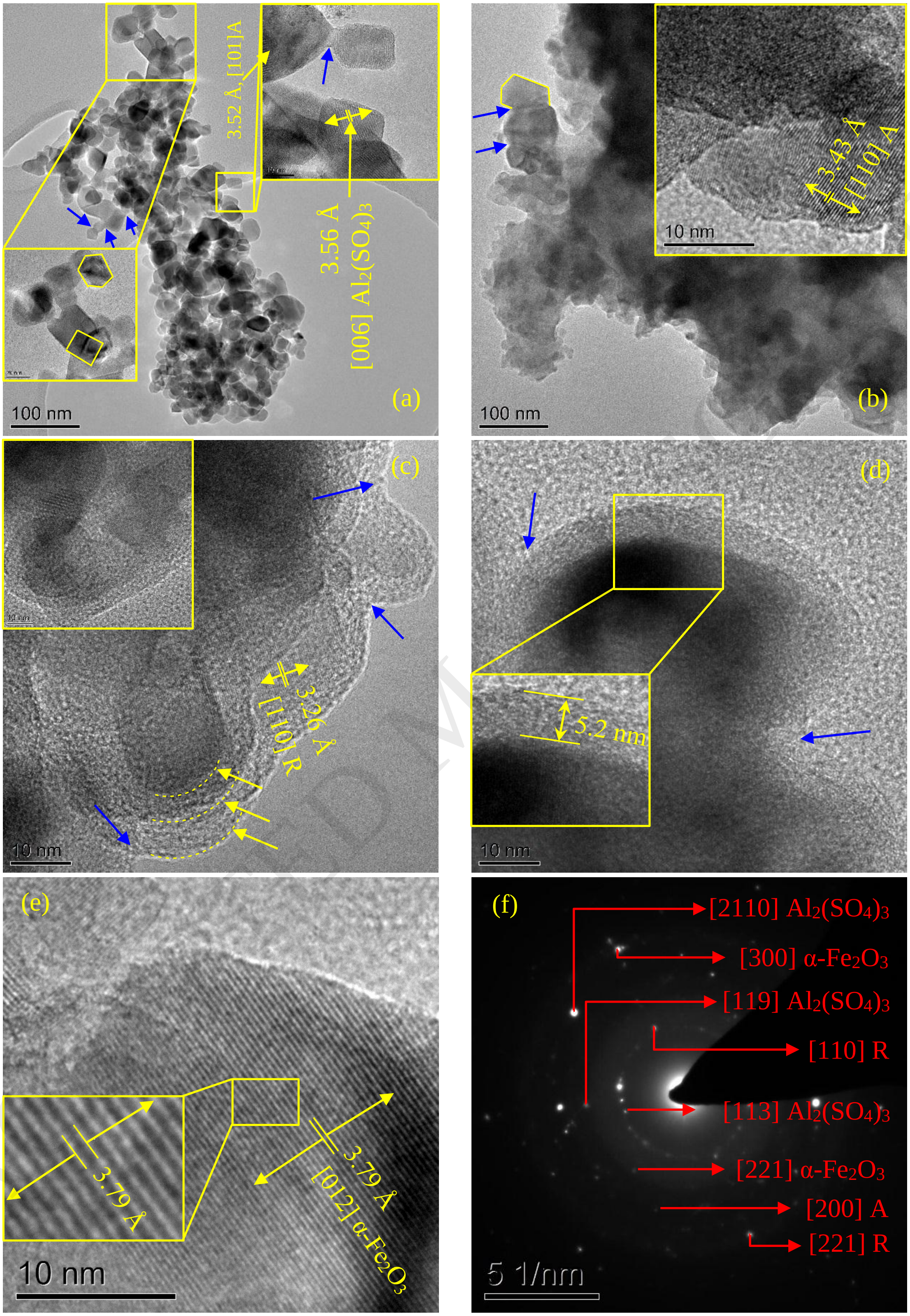

Figure 4. (a-e) TEM images and (f) SAED of SO_4/Fe-Al-TiO_2

EDS confirms the presence of O, S, Fe, Al and Ti (**Figure S8-9** and **Table 3**) in the SO_4/Fe-Al-TiO_2 with S uniformly distributed across the material (**Figure S9**).

Table 3. Elemental analysis of SO_4/Fe-Al-TiO_2 by EDS

Element	O	Al	S	Ti	Fe
Weight%	42.2	14.2	7.6	15.0	21.0
Atomic%	64.0	13.3	5.1	8.0	9.6

3.1.2 Surface functionality

The nature of surface sulphoxy species arising from sulfonation was explored by attenuated total reflection (ATR)-FTIR (**Figure 5**). Comparison with the parent Fe-Al-TiO_2 spectrum reveals that sulfonation results in the appearance of new bands characteristic of sulphate groups, with strong peaks at 980, 1065 and 1138 cm^{-1} assigned to S-O stretches of sulfated metal oxides [19, 53-55], and peaks at 1430 and 1469 cm^{-1} attributed to S=O asymmetric and symmetric sulfate stretches respectively. These features are consistent with polynuclear sulphates $S_2O_7^{2-}$ or $S_3O_{10}^{2-}$ [56], presumably arising from the chlorosulfonic acid dimerization (**Figure S10**) prior to surface sulfation. The bands in the region of ~550 to 780 cm^{-1} in Fe-Al-TiO_2 and SO_4/Fe-Al-TiO_2 likely arise from M-O-M bridging stretches [30, 57], and the broad band between 3050-3800 cm^{-1} to surface surface hydroxyls [20, 39, 55, 58] whose presence has been reported to enhance catalytic activity [59]. FTIR thus confirms successful sulfation of Fe-Al-TiO_2 particles.

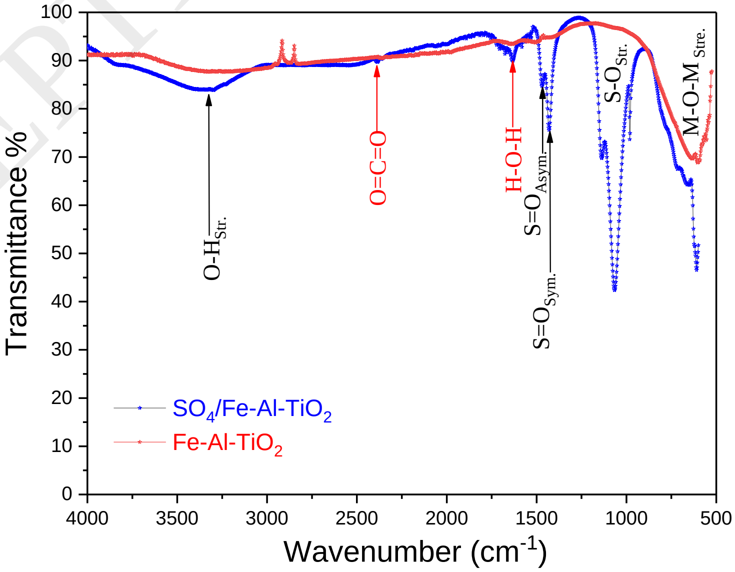

Figure 5. FTIR spectra of Fe-Al-TiO_2 and SO_4/Fe-Al-TiO_2

3.1.3 Textural properties

Nitrogen adsorption/desorption isotherms and corresponding pore size and pore volume distributions are shown in **Figure 6** for the parent TiO_2 NPs, and for the functionalised Al-TiO_2, Fe-Al-TiO_2 and SO_4/Fe-Al-TiO_2 materials. Except for the Fe-Al-TiO_2 sample, the materials all exhibited type II adsorption-desorption isotherms characteristic of macroporous materials (or non-porous materials possessing large interparticle voids). The BET surface areas spanned 49-78 m^2.g^{-1} (**Table S1**) similar to that of the parent titania nanoparticles. All materials exhibited a single hysteresis loop with that for Fe-Al-TiO_2 sample of type II while those of the other materials were of type I [60]. The increase mesoporosity of Fe-Al-TiO_2 suggests that iron functionalisation of the alumina-coated titania NPs creates a highly porous second shell, and/or mesoporous interparticle voids between discrete hematite particles and the Al-TiO_2 nanoparticles.

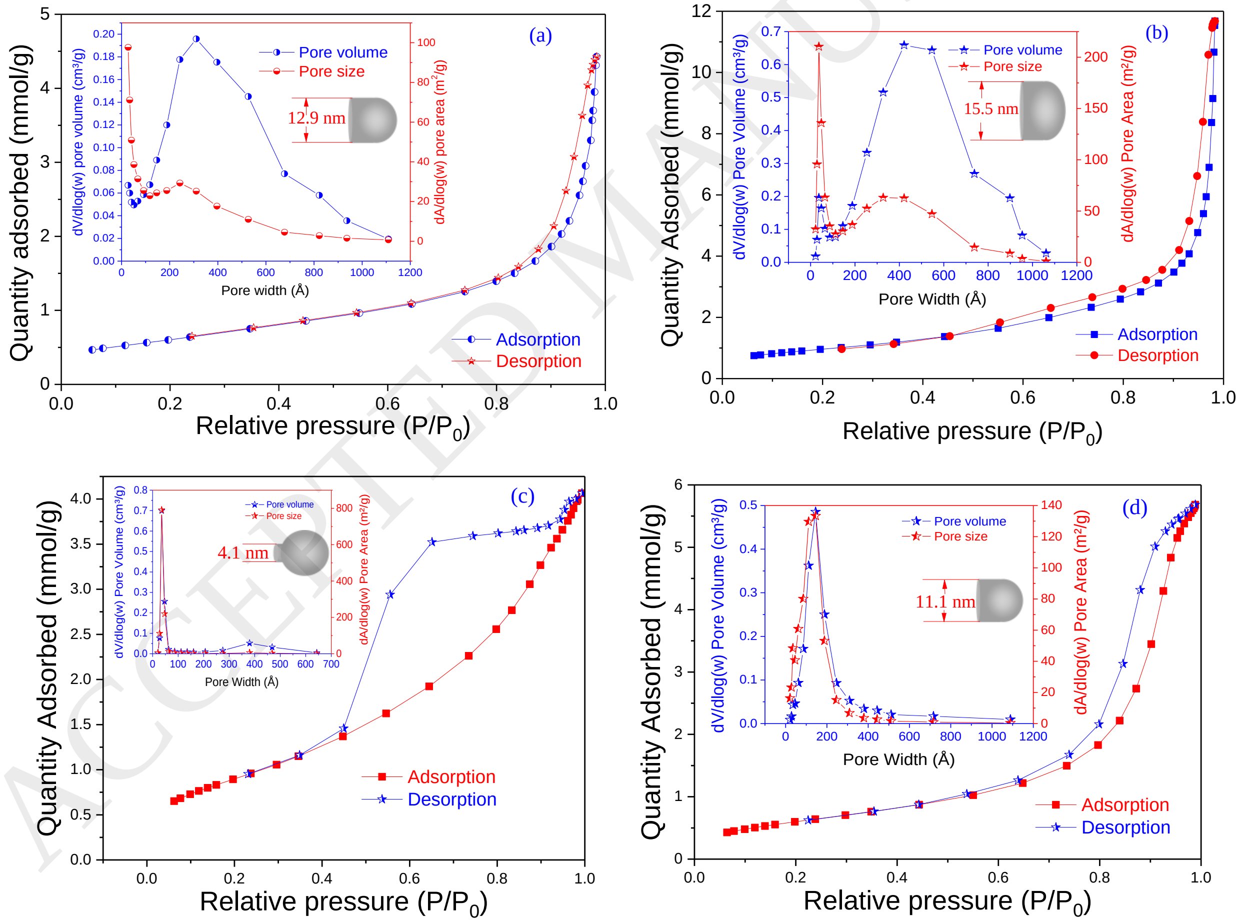

Figure 6. N_2 adsorption-desorption isotherms and total pore volumes with mean pore sizes (inset) for catalysts (a) TiO_2, (b) Al-TiO_2, (c) Fe-Al-TiO_2 and (d) SO_4/Fe-Al-TiO_2

3.1.4 Thermal stability

The TGA profiles of all samples (**Figure 7**) showed only a small weight loss between room temperature and 150 °C due to physisorbed water [18]. No significant further weight losses were observed for any of the samples except for SO_4/Fe-Al-TiO_2 which lost approximately 15 % of the initial total mass above 633 °C due to decomposition of sulphate groups, indicating excellent thermal stability (other sulphated metal oxides are often reported to decompose >430 °C [18, 56].

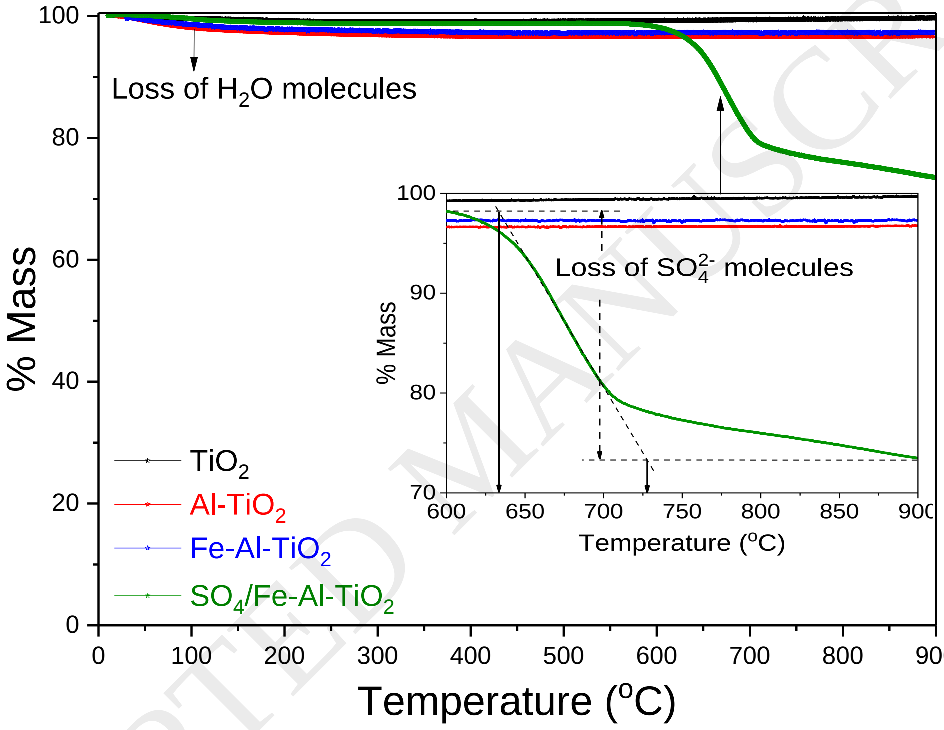

Figure 7. TGA profiles for TiO_2 NPs, Al-TiO_2, Fe-Al-TiO_2 and SO_4/Fe-Al-TiO_2.

3.1.5 Surface acidity

DRIFTS of pyridine titrated materials was employed to quantify their Brønsted/Lewis acid character (**Figure S11**). DRIFT spectra of the samples suggested that all non-sulfonated samples possess a mixture of Lewis and Brønsted acid sites but SO_4/Fe-Al-TiO_2 catalyst is purely Brønsted acidic as shown in **Figure S11**. The shifting of the stretching frequencies of the sulphate groups vibration from Al-TiO_2 and Fe-Al-TiO_2 and SO_4/Fe-Al-TiO_2 indicates stronger interaction between the surface sulphur complex and the adsorbed pyridine molecules. This shifting increases the activity of the catalysts [53]. The mode at 1490 cm^{-1} appeared in all catalyst samples indicating the strong coordination of pyridine and pyridinium ions on the Brønsted and Lewis acid sites, respectively [61]. The ratio of Brønsted to Lewis acid (B/L) sites, extracted from the peak areas of 1541 and 1445 cm^{-1}, for all catalysts are summarised in **Table 4**. Acid loadings were determined from the desorption of reactively-formed propene from n-propylamine saturated TiO_2 and SO_4/Fe-Al-TiO_2 samples (**Figure 8**) and shown in **Table 4**. Sulfation dramatically increased the acid loading relative the parent titania NPs as well as some of this acid loading coming from the acid sites formed by iron oxide or alumina layers [20]. In addition to acting as the catalyst support (nanoparticle core) TiO_2 may also introduce some Lewis acidity to complementing the Brønsted acidity of surface sulfate groups.

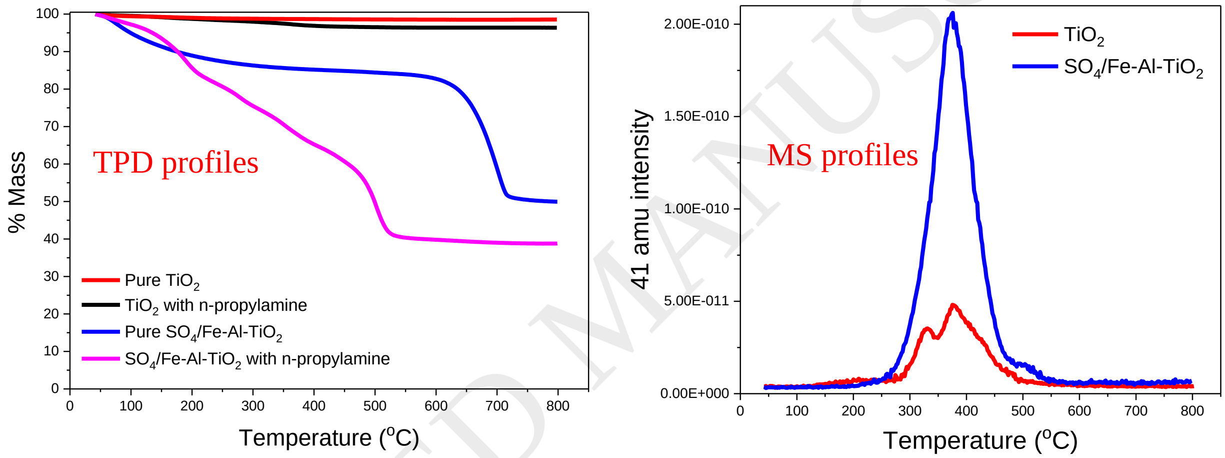

Figure 8. (left) Thermograms, and (right) mass spectra for TiO_2 NPs and SO_4/Fe-Al-TiO_2 of pure and saturated with n-propylamine.

Table 4. Acidic properties of the synthesised materials

Materials	Brønsted:Lewis ratio	Acid loading /mmol.g^{-1}
TiO_2	0.05	0.28
Al-TiO_2	0.33	-
Fe-Al-TiO_2	0.13	-
SO_4/Fe-Al-TiO_2	3.58	1.18

3.1.6 Magnetic properties

The magnetisation curve for SO_4/Fe-Al-TiO_2 was measured at room temperature between 2 and -2 T. The resulting hysteresis loop is shown in **Figure 9**. The magnetic field (M) versus applied magnetic field (H) curve indicates a saturation magnetisation value of the sample at ~10 emu/g. The saturation magnetisation value for pure iron oxide (Fe_2O_3 and Fe_3O_4) is higher than SO_4/Fe-Al-TiO_2. However, SO_4/Fe-Al-TiO_2 still exhibited super paramagnetic behaviour (M_r = 0.65 emu/g and H_c = 0.0024 T as seen in the inset for **Figure 9**) which has been shown sufficient to effect separation of magnetic catalysts from reaction media [45].

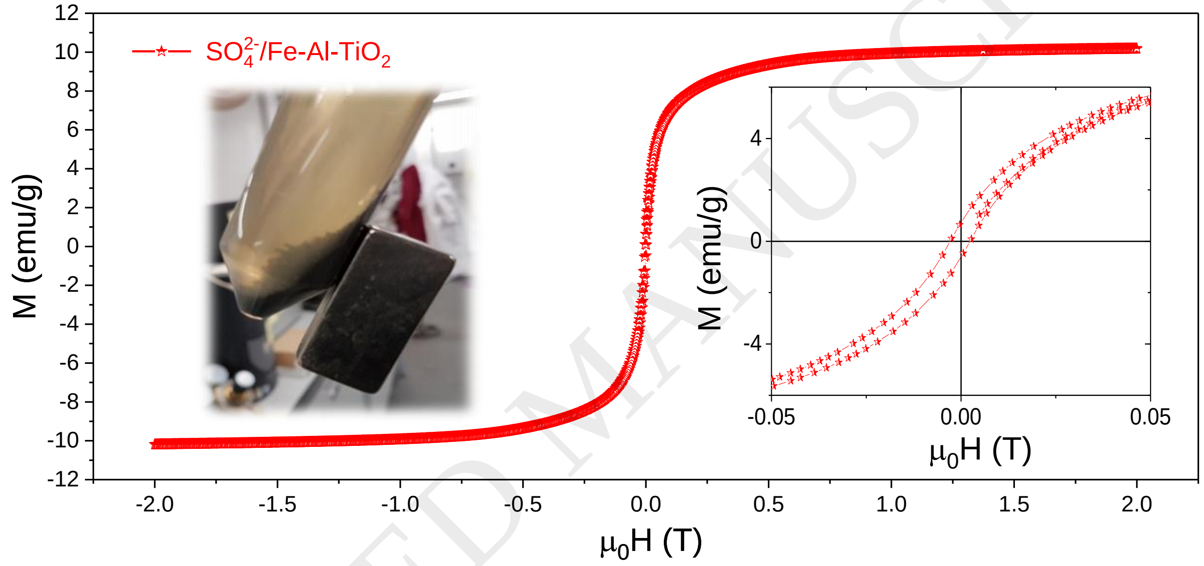

Figure 9. Magnetisation hysteresis loop of SO_4/Fe-Al-TiO_2 at room temperature. (left inset) photograph demonstrating magnetic separation of material from solution, (right inset).

3.2 Catalytic performance

The SO_4/Fe-Al-TiO_2 material was subsequently evaluated for the simultaneous esterification and transesterification of WCO to produce biodiesel. Optimum reaction conditions were explored through examining the impact of methanol:WCO stoichiometry, temperature, and catalyst loading on FAME yield. **Figure 10a** shows the time dependence of FAME production for 1.5 wt% SO_4/Fe-Al-TiO_2, a methanol:WCO molar ratio of 9:1 and reaction temperature of 75 °C (these initial conditions chosen from our previous studies on $Ti(SO_4)O$ catalysts [5]). FAME yield increased linearly with time before reaching a plateau at 83 % after 2.5 h. The effect of catalyst mass was subsequently explored (**Figure 10b**) at a methanol:WCO molar ratio of 9:1 after 2.5 h reaction at

75 °C, with increases between 0.5-1.5 wt% resulting in a linear increase in FAME yield to a maximum of 91 %; additional catalyst loadings had negligible impact. This observation shows that esterification/transesterification were reaction-rate limited for loadings ≤1.5 wt% and that higher loadings are therefore undesirable. Since esterification and transesterification are both reversible, excess methanol is employed to shift the equilibrium reaction towards FAME, with methanol:oil molar ratios between 3-60:1 commonly employed; higher methanol concentrations promote oil solubility and hence FAME yields [62-64].

Figure 10c shows the effect of methanol:WCO ratio with 3 wt% catalyst after 2.5 h reaction at 75 °C. FAME yield was directly proportional to the methanol:WCO ratio between 1:1-10:1, with a limiting value of 92 % again attained. Finally, the impact of reaction temperature was assessed between 25-90 °C (**Figure 10d**) for 3 wt% catalyst and a 10:1 methanol:oil molar ratio after 2.5 h reaction. FAME yield increased continuously for temperatures <75 °C, reaching a limiting value of 95 %, probably reflecting both increased reactant activation and higher oil miscibility [20]. Higher temperatures had negligible impact on FAME production indicating that the reaction had reached equilibrium.

The sensitivity of SO_4/Fe-Al-TiO_2 to FFA within bio-oil feedstocks was also explored by evaluating catalytic performance in the transesterification of a virgin corn oil feedstock deliberately spiked with between 0.5-20 wt% oleic acid (as a model FFA) using the optimum reaction conditions determined above (**Figure 11a**): 3 wt% catalyst loading, 10:1 methanol:oil, and 90 °C after 2.5 h reaction). Surprisingly, the FAME yield remained at 95 % independent of the FFA content of the oil feedstock, indicating a robust catalyst. Catalyst lifetime was also assessed in 10 consecutive reactions (**Figure 11b**) under the same reaction conditions, employing magnetic separation to recover the spent catalyst each time. The spent catalyst was washed repeatedly with a 1:1 vol% methanol:n-hexane mixture to remove any organic residues, and then calcined for 2 h at 250 °C before addition to a fresh reaction mixture. Excellent stability was again evidence by retention of a high (>90 %) FAME yield for 10 recycles. Powder XRD patterns of the spent catalyst after each reaction confirmed retention of the crystalline phases present in the fresh material (**Figure S12**).

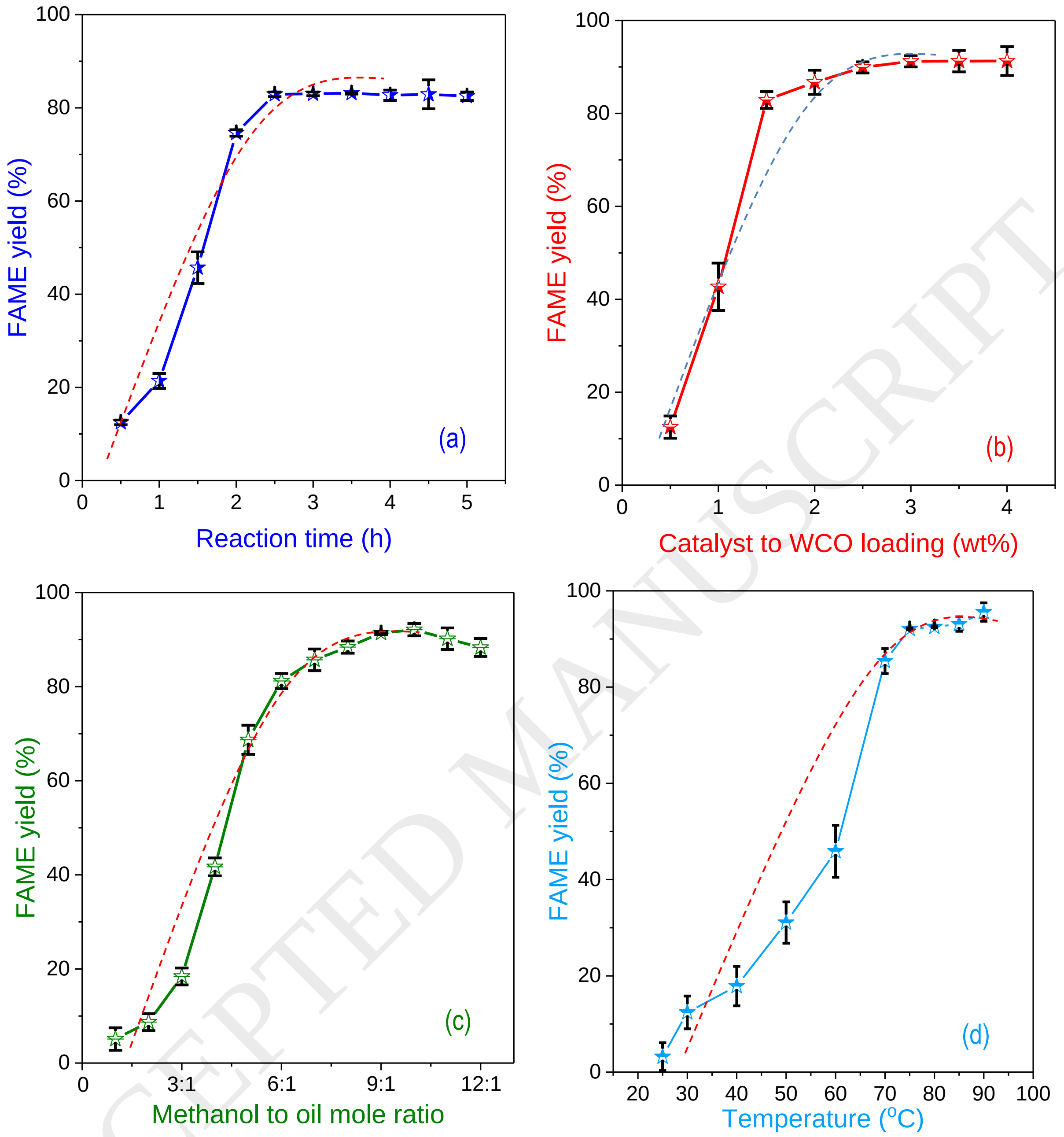

Figure 10. Effects of (a) reaction time, (b) catalyst loading, (c) methanol to WCO molar ratio, and (d) reaction temperature 1on the FAME yield using synthesized SO_4/Fe-Al-TiO_2 catalyst.

Table 5 compares the performance of SO_4/Fe-Al-TiO_2 with some solid acid catalysts from literature, showing that the catalyst synthesized in this study can produce similar amount of FAME (96 % FAME) at much milder reaction temperature and shorter time. Although our previously reported Ti(SO_4)O catalyst gave an excellent 97 % FAME yield from a WCO feedstock under similar reaction conditions (albeit a lower temperature and catalyst loading), this was less robust than the present SO_4/Fe-Al-TiO_2 catalyst, deactivating after 10 recycles due to sulfate leaching. It is also important to note that Ti(SO_4)O was only effective for WCO containing ≤6 wt% FFA, versus 20 wt% for SO_4/Fe-Al-TiO_2. Al and Fe within SO_4/Fe-Al-TiO_2 may inhibit sulfate leaching [65]. In addition to this, water by-product from the esterification of oleic acid (as a model FFA) had no significant impact on the deactivation or poisoning of active sites in the SO_4/Fe-Al-TiO_2 catalyst, and SO_4/Fe-Al-TiO_2 is readily separated from the reaction mixture by an external magnetic field.

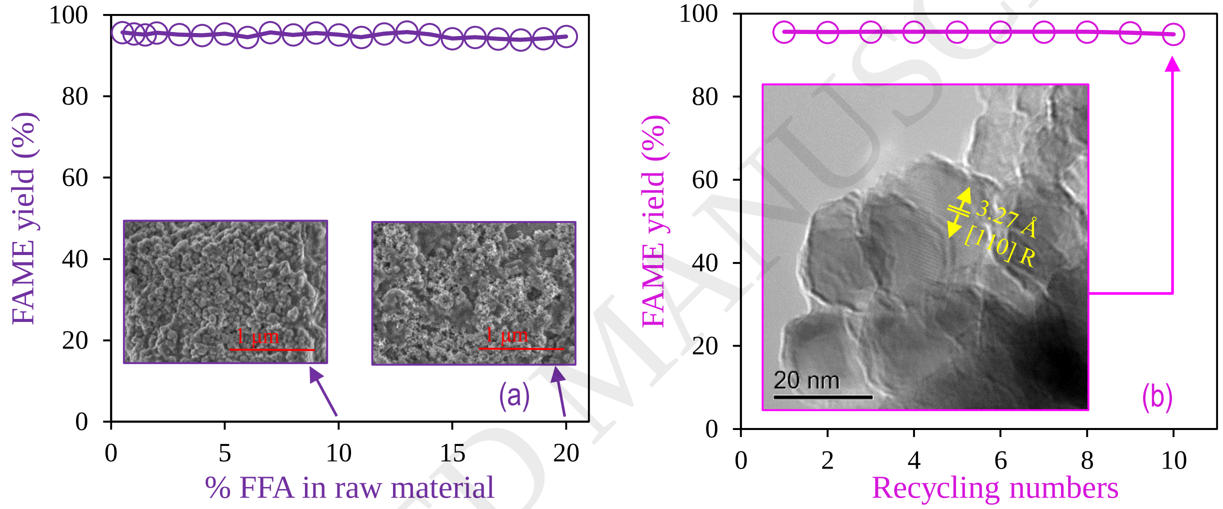

Figure 11. Effect of (a) oleic acid content and (b) recycling of SO_4/Fe-Al-TiO_2 catalyst on the FAME yield. The inset TEM result for the recovered spent catalyst from WCO transesterification process after run 10 shows a clear [110] facets for the rutile TiO_2 NPs (ICDD: 01-076-9000)

Table 5. Comparison of sulfated metal oxide catalysts for biodiesel production from WCO.

	This work	**Gardy et al [5]**	**Alhassan et al [31]**	**Wang et al [66]**
Feedstock	WCO	WCO	WCO	WCO
Methanol:oil ratio	10:1	9:1	20:1	10:1
Catalyst	SO_4/Fe-Al-TiO_2	$Ti(SO_4)O$	Fe_2O_3-MnO-SO_4/ZrO_2	SO_4^{2-}/TiO_2/La^{+3}
Catalyst loading / wt%	3	1.5	3	5
Reaction time / h	2.5	3	6	1
Particle size / nm	47	25	-	-
Surface area / $m^2.g^{-1}$	51	45	72	229
Temperature / °C	90	75	180	110
FAME yield / %	96	97	96	>90
Recycles	10 (94 %)	10 (73 %)	7 (94 %)	5 (90%)

3.3 Biodiesel characterisation

The biodiesel derived from the esterification and transesterification of WCO over SO_4/Fe-Al-TiO_2 was analysed and characterised according to ASTM and/or EN standards and the results summarized in **Table S2** and **Table S3**. The principal FAME components in **Table S2** were methyl palmitate, methyl oleate and methyl linoleate. The physical characteristics of the biodiesel properties conformed with ASTM and EU standards, with a cloud point of -11.3 °C (**Figure S13**). Decomposition/combustion of the synthetic biodiesel occurred >144 °C and was complete by 226 °C (**Figure S14**).

Conclusions

A super paramagnetic solid acid catalyst comprising SO_4/Fe-Al-TiO_2 was prepared by the stepwise functionalise of titania NPs. Extensive characterisation of the catalyst bulk and surface properties revealed it possessed a high acid loading and Brønsted acid character arising from surface sulfate and persulfate species generated by chlorosulfonic acid functionalisation, and strong magnetic character arising from hematite nanoparticle. SO_4/Fe-Al-TiO_2 exhibited promising activity for the (trans)esterification of WCO to biodiesel. Under optimum conditions of 3 wt% catalyst, a 10:1

molar ratio of methanol:WCO molar and 90 °C, a 95.6% FAME yield was attained after 2.5 h reaction. The SO_4/Fe-Al-TiO_2 catalyst exhibited excellent stability and recyclability employing magnetic separation and thermal regeneration, maintaining a high performance for virgin corn oil transesterification even in the presence of up to 20 wt% oleic acid, and for over 10 consecutive reactions cycles with WCO.

Conflicts of interest

The authors declare no conflict of interest.

Acknowledgments

The authors are grateful to Dr Adrian Cunliffe, Dr Zabeada Aslam, Dr Faye Esat, Dr Ben Douglas and Mr. Stuart Micklethwaite for their technical assistance.

References

1. Armaroli, N. and V. Balzani, *The future of energy supply: challenges and opportunities.* Angewandte Chemie International Edition, **2007**. 46(1-2): p. 52-66.
2. Rehan, M., J. Gardy, A. Demirbas, U. Rashid, W. Budzianowski, D. Pant, and A. Nizami, *Waste to biodiesel: A preliminary assessment for Saudi Arabia.* Bioresource technology, **2018**. 250: p. 17-25.
3. Dacquin, J.-P., A.F. Lee, C. Pirez, and K. Wilson, *Pore-expanded SBA-15 sulfonic acid silicas for biodiesel synthesis.* Chemical Communications, **2012**. 48(2): p. 212-214.
4. Gardy, J., A. Hassanpour, X. Lai, and M. Rehan, *The influence of blending process on the quality of rapeseed oil-used cooking oil biodiesels.* International Scientific Journal (Journal of Environmental Science). **2014**. 3: p. 233-240.
5. Gardy, J., A. Hassanpour, X. Lai, and M.H. Ahmed, *Synthesis of Ti(SO_4)O solid acid nano-catalyst and its application for biodiesel production from used cooking oil.* Applied Catalysis A: General, **2016**. 527: p. 81–95.
6. Salam, K.A., S.B. Velasquez-Orta, and A.P. Harvey, *A sustainable integrated in situ transesterification of microalgae for biodiesel production and associated co- products- A review.* Renewable and Sustainable Energy Reviews, **2016**. 65: p. 1179-1198.
7. Gude, V.G. and G.E. Grant, *Biodiesel from waste cooking oils via direct sonication.* Applied Energy, **2013**. 109: p. 135-144.
8. Wahidin, S., A. Idris, and S.R.M. Shaleh, *Rapid biodiesel production using wet microalgae via microwave irradiation.* Energy Conversion and Management, **2014**. 84: p. 227-233.
9. Shuit, S.H., K.T. Lee, A.H. Kamaruddin, and S. Yusup, *Reactive extraction and in situ esterification of Jatropha curcas L. seeds for the production of biodiesel.* Fuel, **2010**. 89(2): p. 527-530.
10. Jitputti, J., B. Kitiyanan, P. Rangsunvigit, K. Bunyakiat, L. Attanatho, and P. Jenvanitpanjakul, *Transesterification of crude palm kernel oil and crude coconut oil by different solid catalysts.* Chemical Engineering Journal, **2006**. 116(1): p. 61-66.
11. Rattanaphra, D., A. Harvey, and P. Srinophakun, *Simultaneous conversion of triglyceride/free fatty acid mixtures into biodiesel using sulfated zirconia.* Topics in Catalysis, **2010**. 53(11-12): p. 773-782.
12. Gardy, J., *Biodiesel production from used cooking oil using novel solid acid catalysts*, in *School of Chemical and Process Engineering*. **2017**, University of Leeds: United Kingdom, Leeds, White Rose etheses.
13. Lee, A.F., J.A. Bennett, J.C. Manayil, and K. Wilson, *Heterogeneous catalysis for sustainable biodiesel production via esterification and transesterification.* Chemical Society Reviews, **2014**. 43(22): p. 7887-7916.
14. Manayil, J.C., C.V. Inocencio, A.F. Lee, and K. Wilson, *Mesoporous sulfonic acid silicas for pyrolysis bio-oil upgrading via acetic acid esterification.* Green Chemistry, **2016**. 18(5): p. 1387-1394.
15. Guldhe, A., P. Singh, F.A. Ansari, B. Singh, and F. Bux, *Biodiesel synthesis from microalgal lipids using tungstated zirconia as a heterogeneous acid catalyst and its comparison with homogeneous acid and enzyme catalysts.* Fuel, **2017**. 187: p. 180-188.
16. Gardy, J., A. Hassanpour, X. Lai, M.H. Ahmed, and M. Rehan, *Biodiesel production from used cooking oil using a novel surface functionalised TiO_2 nano-catalyst.* Applied Catalysis B: Environmental, **2017**. 207: p. 297-310.

17. Furuta, S., H. Matsuhashi, and K. Arata, *Biodiesel fuel production with solid amorphous-zirconia catalysis in fixed bed reactor.* Biomass and Bioenergy, **2006**. 30(10): p. 870-873.
18. Wang, J., P. Yang, M. Fan, W. Yu, X. Jing, M. Zhang, and X. Duan, *Preparation and characterization of novel magnetic* $ZrO_2/TiO_2/Fe_3O_4$ *solid superacid.* Materials letters, **2007**. 61(11): p. 2235-2238.
19. De Almeida, R.M., L.K. Noda, N.S. Gonçalves, S.M. Meneghetti, and M.R. Meneghetti, *Transesterification reaction of vegetable oils, using superacid sulfated* TiO_2*–base catalysts.* Applied Catalysis A: General, **2008**. 347(1): p. 100-105.
20. Lam, M.K., K.T. Lee, and A.R. Mohamed, *Sulfated tin oxide as solid superacid catalyst for transesterification of waste cooking oil: an optimization study.* Applied Catalysis B: Environmental, **2009**. 93(1): p. 134-139.
21. Jenie, A., D.S. Kusuma, A. Kristiani, J.A. Laksmono, and S. Tursiloadi, *Preparation and characterization of sulfated titania catalysts for the isomerisation of citronellal.* International Journal of Basic & Applied Sciences IJBAS-IJENS, **2010**. 10(06): p. 5-10.
22. Guan, D., M. Fan, J. Wang, Y. Zhang, Q. Liu, and X. Jing, *Synthesis and properties of magnetic solid superacid:* $SO_4^{2-}/ZrO_2–B_2O_3–Fe_3O_4$*.* Materials Chemistry and Physics, **2010**. 122(1): p. 278-283.
23. Wen, Z., X. Yu, S.-T. Tu, J. Yan, and E. Dahlquist, *Biodiesel production from waste cooking oil catalyzed by* TiO_2*–MgO mixed oxides.* Bioresource technology, **2010**. 101(24): p. 9570-9576.
24. Li, Y., X.-D. Zhang, L. Sun, M. Xu, W.-G. Zhou, and X.-H. Liang, *Solid superacid catalyzed fatty acid methyl esters production from acid oil.* Applied Energy, **2010**. 87(7): p. 2369-2373.
25. Valle-Vigón, P., M. Sevilla, and A.B. Fuertes, *Sulfonated mesoporous silica–carbon composites and their use as solid acid catalysts.* Applied Surface Science, **2012**. 261: p. 574-583.
26. Shen, J., Y. Zhu, X. Yang, and C. Li, *Magnetic composite microspheres with exposed {001} faceted* TiO_2 *shells: a highly active and selective visible-light photocatalyst.* Journal of Materials Chemistry, **2012**. 22(26): p. 13341-13347.
27. Madhuvilakku, R. and S. Piraman, *Biodiesel synthesis by* TiO_2*–ZnO mixed oxide nanocatalyst catalyzed palm oil transesterification process.* Bioresource technology, **2013**. 150: p. 55-59.
28. Qin, S., W. Cai, X. Tang, and L. Yang, *Sensitively monitoring photodegradation process of organic dye molecules by surface-enhanced Raman spectroscopy based on* $Fe_3O_4@SiO_2@TiO_2@Ag$ *particle.* Analyst, **2014**. 139(21): p. 5509-5515.
29. Osatiashtiani, A., A.F. Lee, D.R. Brown, J.A. Melero, G. Morales, and K. Wilson, *Bifunctional* SO_4^{2-}/ZrO_2 *catalysts for 5-hydroxymethylfufural (5-HMF) production from glucose.* Catalysis Science & Technology, **2014**. 4(2): p. 333-342.
30. Li, C., J. Tan, X. Fan, B. Zhang, H. Zhang, and Q. Zhang, *Magnetically separable one dimensional* $Fe_3O_4/P(MAA-DVB)/TiO_2$ *nanochains: preparation, characterization and photocatalytic activity.* Ceramics International, **2015**. 41(3): p. 3860-3868.
31. Alhassan, F.H., U. Rashid, and Y. Taufiq-Yap, *Synthesis of waste cooking oil-based biodiesel via effectual recyclable bi-functional* Fe_2O_3*-MnO-*SO_4^{2-}/ZrO_2 *nanoparticle solid catalyst.* Fuel, **2015**. 142: p. 38-45.
32. Raia, R.Z., L.S. da Silva, S.M.P. Marcucci, and P.A. Arroyo, *Biodiesel production from Jatropha curcas L. oil by simultaneous esterification and transesterification using sulphated zirconia.* Catalysis Today, **2016**.

33. Osatiashtiani, A., L.J. Durndell, J.C. Manayil, A.F. Lee, and K. Wilson, *Influence of alkyl chain length on sulfated zirconia catalysed batch and continuous esterification of carboxylic acids by light alcohols.* Green Chemistry, **2016**. 18(20): p. 5529-5535.
34. Noda, L.K., R.M. de Almeida, N.S. Gonçalves, L.F.D. Probst, and O. Sala, *TiO_2 with a high sulfate content—thermogravimetric analysis, determination of acid sites by infrared spectroscopy and catalytic activity.* Catalysis today, **2003**. 85(1): p. 69-74.
35. Zhang, H., H. Yu, A. Zheng, S. Li, W. Shen, and F. Deng, *Reactivity Enhancement of 2-Propanol Photocatalysis on SO_4^{2-}/TiO_2: Insights from Solid-State NMR Spectroscopy.* Environmental science & technology, **2008**. 42(14): p. 5316-5321.
36. Li, Z., R. Wnetrzak, W. Kwapinski, and J.J. Leahy, *Synthesis and characterization of sulfated TiO_2 nanorods and ZrO_2/TiO_2 nanocomposites for the esterification of biobased organic acid.* ACS applied materials & interfaces, **2012**. 4(9): p. 4499-4505.
37. Jiang, Y.-X., X.-M. Chen, Y.-F. Mo, and Z.-F. Tong, *Preparation and properties of Al-PILC supported SO_4^{2-}/TiO_2 superacid catalyst.* Journal of Molecular Catalysis A: Chemical, **2004**. 213(2): p. 231-234.
38. Lai, D.-m., L. Deng, Q.-x. Guo, and Y. Fu, *Hydrolysis of biomass by magnetic solid acid.* Energy & Environmental Science, **2011**. 4(9): p. 3552-3557.
39. Wu, L., Y. Zhou, W. Nie, L. Song, and P. Chen, *Synthesis of highly monodispersed teardrop-shaped core–shell SiO_2/TiO_2 nanoparticles and their photocatalytic activities.* Applied Surface Science, **2015**. 351: p. 320-326.
40. Jacinto, M.J., O.H. Santos, R.F. Jardim, R. Landers, and L.M. Rossi, *Preparation of recoverable Ru catalysts for liquid-phase oxidation and hydrogenation reactions.* Applied Catalysis A: General, **2009**. 360(2): p. 177-182.
41. Lu, A.H., E.e.L. Salabas, and F. Schüth, *Magnetic nanoparticles: synthesis, protection, functionalization, and application.* Angewandte Chemie International Edition, **2007**. 46(8): p. 1222-1244.
42. Sobhani, S., Z.P. Parizi, and N. Razavi, *Nano n-propylsulfonated γ-Fe_2O_3 as magnetically recyclable heterogeneous catalyst for the efficient synthesis of β-phosphonomalonates.* Applied Catalysis A: General, **2011**. 409: p. 162-166.
43. Tang, S., L. Wang, Y. Zhang, S. Li, S. Tian, and B. Wang, *Study on preparation of Ca/Al/Fe3O4 magnetic composite solid catalyst and its application in biodiesel transesterification.* Fuel Processing Technology, **2012**. 95: p. 84-89.
44. Xin, T., M. Ma, H. Zhang, J. Gu, S. Wang, M. Liu, and Q. Zhang, *A facile approach for the synthesis of magnetic separable Fe_3O_4@ TiO_2, core–shell nanocomposites as highly recyclable photocatalysts.* Applied Surface Science, **2014**. 288: p. 51-59.
45. Moghanian, H., A. Mobinikhaledi, A. Blackman, and E. Sarough-Farahani, *Sulfanilic acid-functionalized silica-coated magnetite nanoparticles as an efficient, reusable and magnetically separable catalyst for the solvent-free synthesis of 1-amido-and 1-aminoalkyl-2-naphthols.* RSC Advances, **2014**. 4(54): p. 28176-28185.
46. Zabeti, M., W.M.A.W. Daud, and M.K. Aroua, *Activity of solid catalysts for biodiesel production: a review.* Fuel Processing Technology, **2009**. 90(6): p. 770-777.
47. Anuradha, S., K. Raj, V. Vijayaraghavan, and B. Viswanathan, *Sulphated Fe_2O_3-TiO_2 catalysed transesterification of soybean oil to biodiesel.* Indian Journal of Chemistry **2014**. 53A: p. 1493-1499.

48. Bhongsuwan, T., D. Bhongsuwan, N. Chomchoey, and L. Boonchuay, *Effect of calcination temperature in production of magnetic nanoparticles for arsenic adsorption.* Mater. Chem. Phys, **2008**. 110(2-3): p. 426-433.
49. Massart, R., *Preparation of aqueous magnetic liquids in alkaline and acidic media.* IEEE transactions on magnetics, **1981**. 17(2): p. 1247-1248.
50. Hanaor, D.A. and C.C. Sorrell, *Review of the anatase to rutile phase transformation.* Journal of Materials science, **2011**. 46(4): p. 855-874.
51. ASTM-D974, *Standard test method for acid and base number by colour-indicator titration.* **2012**: p. 1-7.
52. EN-14104, *Fat and oil derivatives-fatty acid methyl esters (FAME): determination of acid value.* **2003**.
53. Jin, T., T. Yamaguchi, and K. Tanabe, *Mechanism of acidity generation on sulfur-promoted metal oxides.* The Journal of Physical Chemistry, **1986**. 90(20): p. 4794-4796.
54. Noda, L.K., R.M. de Almeida, L.F.D. Probst, and N.S. Gonçalves, *Characterization of sulfated* TiO_2 *prepared by the sol–gel method and its catalytic activity in the n-hexane isomerization reaction.* Journal of Molecular Catalysis A: Chemical, **2005**. 225(1): p. 39-46.
55. Ropero-Vega, J., A. Aldana-Pérez, R. Gómez, and M. Niño-Gómez, *Sulfated titania* $[TiO_2/SO_4^{\ 2-}]$*: A very active solid acid catalyst for the esterification of free fatty acids with ethanol.* Applied Catalysis A: General, **2010**. 379(1): p. 24-29.
56. Smith, Y.R., K.J.A. Raj, V.R. Subramanian, and B. Viswanathan, *Sulfated* Fe_2O_3*–*TiO_2 *synthesized from ilmenite ore: a visible light active photocatalyst.* Colloids and Surfaces A: Physicochemical and Engineering Aspects, **2010**. 367(1): p. 140-147.
57. Naeimi, H. and Z.S. Nazifi, *A highly efficient nano-*Fe_3O_4 *encapsulated-silica particles bearing sulfonic acid groups as a solid acid catalyst for synthesis of 1, 8-dioxo-octahydroxanthene derivatives.* Journal of Nanoparticle Research, **2013**. 15(11): p. 2026.
58. Jafar Tafreshi, M. and Z. Masoomi Khanghah, *Infrared spectroscopy studies on sol-gel prepared alumina powders.* Materials Science, **2015**. 21(1): p. 28-31.
59. Park, Y.-M., D.-W. Lee, D.-K. Kim, J.-S. Lee, and K.-Y. Lee, *The heterogeneous catalyst system for the continuous conversion of free fatty acids in used vegetable oils for the production of biodiesel.* Catalysis Today, **2008**. 131(1): p. 238-243.
60. Klobes, P., K. Meyer, and R.G. Munro, *Porosity and specific surface area measurements for solid materials*. Vol. Special publication 960-17. **2006**, US, Washington: US Department of Commerce, Technology Administration, National Institute of Standards and Technology. 88.
61. Tao, M., L. Xue, Z. Sun, S. Wang, X. Wang, and J. Shi, *Tailoring the synergistic Brønsted-Lewis acidic effects in heteropolyacid catalysts: applied in esterification and transesterification reactions.* Scientific reports, **2015**. 5.
62. Leclercq, E., A. Finiels, and C. Moreau, *Transesterification of rapeseed oil in the presence of basic zeolites and related solid catalysts.* Journal of the American Oil Chemists' Society, **2001**. 78(11): p. 1161-1165.
63. Furuta, S., H. Matsuhashi, and K. Arata, *Biodiesel fuel production with solid superacid catalysis in fixed bed reactor under atmospheric pressure.* Catalysis communications, **2004**. 5(12): p. 721-723.
64. Shu, Q., J. Gao, Z. Nawaz, Y. Liao, D. Wang, and J. Wang, *Synthesis of biodiesel from waste vegetable oil with large amounts of free fatty acids using a carbon-based solid acid catalyst.* Applied Energy, **2010**. 87(8): p. 2589-2596.

65. Anuradha, S., K. Raj, V. Vijayaraghavan, and B. Viswanathan, *Sulphated* Fe_2O_3-TiO_2 *catalysed transesterification of soybean oil to biodiesel.* Indian Journal of Chemistry, **2014**. 53A: p. 1493-1499.
66. Wang, K., J. Jiang, Z. Si, and X. Liang, *Biodiesel production from waste cooking oil catalyzed by solid acid* $SO_4^{2-}/TiO_2/La^{3+}$. Journal of Renewable and Sustainable Energy, **2013**. 5(5): p. 052001.